JOURNAL OF AIRCRAFT
Vol. 44, No. 4, July–August 2007

Influence of Vortex Core on Wake Vortex Sound Emission

Z. C. Zheng* and Wenhua Li†
Kansas State University, Manhattan, Kansas 66506
and
F. Y. Wang‡ and H. Wassaf§
John A. Volpe National Transportation Systems Center, Cambridge, Massachusetts 02142

DOI: 10.2514/1.27077

A possible sound emission mechanism of aircraft wake vortices has been identified by using both measurement data and theoretical results. This mechanism relates consistently to a dominant frequency of sound pressure matching the rotation frequency of a Kirchhoff vortex. The rotation of the Kirchhoff vortex is due to the self-induction inside the vortex core. Numerical simulations are necessary for a more realistic wake consisting of a counterrotating vortex pair with inviscid ground effects and shear flow. The simulations are carried out using a vortex particle method. A far-field vortex sound formulation, based on asymptotic expansions, is developed to calculate acoustic pressure from the wake vortices. The simulation results confirm that the frequency of the wake sound emission is essentially the same as the classical Kirchhoff vortex, even under the influences of an inviscid ground effect or a weak-shear cross wind. The aforementioned results suggest that the identified mechanism should be fairly robust, which demonstrates its persistency under several different environmental conditions.

I. Introduction

FUNDAMENTALLY, predicting the dynamics of aircraft wake vortices is one of the remaining challenges in unsteady, high-Reynolds-number fluid mechanics problems. Operationally, wake vortices pose both safety and capacity concerns that directly affect airport transportation. Wake encounters potentially could impose severe flight control demands in aircraft that are flying in limited airspace. The need to avoid such encounters is a primary consideration in controlling aircraft spacing specifications around congested airports [1,2]. If the aircraft spacing specifications are too conservative, substantial reductions in passenger throughput result at busy airports. On the other hand, if the spacing standards are overly optimistic, potential dangerous vortex encounters can occur.

Previous efforts in wake vortex research were concerned with developing engineering prediction models for the wake vortex behavior in response to weather conditions in the lower atmosphere [3–8]. More recently, a scheme for actively monitoring wake vortices has emerged by passively tracking the acoustic emissions from wake vortices [9], similar to the concept of using acoustic energy to monitor severe weather and tornadoes [10]. This possibility is currently under examination. For that purpose, the key questions that need to be answered are as follows: 1) Do wake vortices generate sound every time? 2) If so, is the generated acoustic signal consistent and measurable, which contains diagnostic information to indicate the state of the vortex system?

The answer to the first question should be positive from the point of view of fluid dynamics and aeroacoustics. This is because many observations of wake vortex sound have been made under a variety of conditions and the flow related to wake vortices is highly unsteady: the unsteady motion of the vortices, vortex decay, vortex instabilities and breakdown, wake interactions with the ambient turbulence and stratification, ground effects, etc. Because of all of the unsteadiness in the flowfield, the expectation is that sound emission would be unavoidable from wake vortices. With various scales at which these multiple vortices interact with each other, it may also be anticipated that the measured acoustic spectra emitted from the trailing wake would be broadband.

Now the difficult part is the second question. The airspace around an airport is a quite noisy environment. Noise sources include those from engines, airframes, and the atmosphere (such as wind noise), in addition to all the vortex wakes from airplanes in the terminal area air traffic. Therefore, the second question should be answered from the perspective of what is unique to the wake vortex sound, in both the signal patterns and source mechanisms, as well as in the relation between the two. For the purpose of identifying a unique sound source mechanism, all of the unsteady flow structures mentioned in the preceding paragraph could be candidates because each of them represents a unique fluid dynamic aspect pertaining to wake vortices. However, not all of them are capable of generating a reliable, repeatable, and detectable acoustic signal. The studies to date have focused on experimental characterization [11–18], and a rigorous analytical identification of the noise source that is consistent and unique to aircraft vortices is lacking. We have started theoretical investigations on sound generation mechanisms to identify consistent components of wake vortex noise.

There are only two ways to make a vortex system to emit sound: unsteady motion of the vortices or change of strength [19]. The internal decay of a vortex due to viscous and turbulent effects is a very slow process in a realistic high-Reynolds-number environment, such as the environment for the aircraft wake vortex system. With external influences such as background turbulence and stratification, the decay process can be sped up [20] and, at the same time, be oscillatory. A previous study shows that the related sound emission can peak at a frequency that is dependent on the circulation fluctuations and the vortex decay coefficient [21]. Because of the low-frequency nature of the background turbulence and stratification, this provides a possible mechanism for broadband, low-frequency vortex sound emission. However, field measurements

Presented as Paper 2538 at the 12th AIAA/CEAS Aeroacoustics Conference, Cambridge, MA, 8–10 May 2006; received 16 August 2006; revision received 1 December 2006; accepted for publication 7 January 2007.

*Associate Professor, Department of Mechanical and Nuclear Engineering. Senior Member AIAA.
†Graduate Research Assistant, Department of Mechanical and Nuclear Engineering.
‡Aerospace Engineer, Advanced Communication, Navigation and Surveillance Division, RTV-4A. Senior Member AIAA.
§Electronics Engineer, Advanced Communication, Navigation and Surveillance Division, RTV-4A.

showed higher frequency contents (e.g., 20–300 Hz) from an aircraft wake vortex [12,15,18], even when the vortex is out of ground effect.

This research is intended to identify the source of the high-frequency sound from an isolated vortex system that includes out-of-ground aircraft wake vortices and wake vortices in inviscid ground effects. Whereas the currently identified decay mechanisms only produce low-frequency sound, the higher-frequency emission source is thus attributed to the unsteady vortex motion. Tang and Ko [22,23] identified two independent types of unsteady vortex motion that radiate sound: the vortex centroid dynamics and the smaller-scale vortex core dynamics. Their analysis showed that the vortex-core deformation tends to generate more high-frequency sound than the vortex centroid dynamics. Tang and Ko and others [24–26] focused their studies on vortex systems in which the unsteady vortex motions are due to leapfrogging, collision, or coalescence. These types of vortex interactions rarely happen in a fully developed aircraft vortex wake, probably not until the Crow instability [27] occurs, leading to demise of wake vortices. Therefore during the life time of a long-lived wake vortex system, the primary vortex-core dynamics is not driven by any of the aforementioned interactions. Rather, the unsteady core dynamics depends on the initial eccentricity during the rollup process, the background shear, and the ground boundary effect. Addressing these issues is the concentration of the current study. A Kirchhoff spinning-core vortex [28] model is thus used as a starting point.

There may exist interactions between the wake vortex systems and ambient turbulence that can sometimes be modeled as a primary vortex structure interacting with a secondary vortex structure. The ground effect, which possibly causes very low-frequency sound emission with the vortex translational acceleration in an inviscid manner [9], is still able to produce complex unsteady fluctuations due to vortex-induced ground-boundary-layer separation and thus needs to be considered. Compressibility can also contribute to the vortex-core dynamics [24]. In addition, sinusoidal and eigenoscillation instabilities can also occur in the short wave form [29–32] whose wave number can be up to eight times that of the Crow instability. But the associated sound is also of lower frequency than that observed experimentally. These effects on vortex sound emission still need to be analyzed.

The analytical solution of the Kirchhoff vortex model only applies to a single vortex in an infinite domain. Aircraft vortex wakes actually consist of a pair of counterrotating vortices. In addition, ground effects and atmospheric conditions also need to be considered. To demonstrate that the Kirchhoff frequency will persist in practical vortex wakes, numerical solutions are needed. In this study, a vortex particle method [33] is used to simulate the vortex-core dynamics in 2-D, inviscid, and incompressible flow. This is particularly suitable for a wake vortex system that is slowly varying in the axial direction, and is of high Reynolds number and low Mach number. A far-field vortex sound formula based on matched asymptotic expansions is then used to relate sound emission to the vortex-core dynamics.

II. Sound Emission from a Spinning Kirchhoff Vortex Core

The Kirchoff vortex is a patch of constant vorticity inside an ellipse and zero vorticity outside. It is an exact solution of the 2-D, incompressible, and inviscid flow equations [28]. An almost circular Kirchhoff vortex has the ellipse defined by the polar equation for the radius of the vortex core:

$$r_K = a[1 + \epsilon \cos(2\theta - \Omega t/2)] \tag{1}$$

where the long axis of the ellipse is $a(1+\epsilon)$, the short axis is $a(1-\epsilon)$, $\epsilon \ll 1$, and Ω is the uniform vorticity in the core. Howe [34] gave the acoustic pressure at $\Omega r/c_o \to \infty$ as

$$p = -\frac{\epsilon}{8}\sqrt{\frac{2\pi a}{r}}\rho_o U^2 M^{3/2} \cos\left[2\theta - \frac{\Omega}{2}\left(t - \frac{r}{c_o} + \frac{\pi}{4}\right)\right] \tag{2}$$

where c_o is the speed of sound, $U = a\Omega/2$, $M = U/c_o$, and r is the radius of far-field acoustic receiver location. The ellipse rotates at an angular velocity of $\Omega/4$, which generates a quadrupole-type sound at a frequency of $\Omega/4\pi$, as shown in Eq. (2). Equation (2) also shows that for $\epsilon = 0$, which is the case of a circular vortex patch in an unbounded potential flow, for example, a Rankine vortex [30], there is no emission because of the steady-state flow produced by a Rankine vortex. In the wake vortex system, the eccentricity is produced during the initial rollup process. An elliptical vortex resulting from shear-layer instability is an evidence [35], because a major portion of the vortex wake is from the wing tip vortices resulting from a primary process of shear-layer instability. Other external effects such as wind shear or turbulence can also cause eccentricity in a wake vortex.

The analytical solution for the flowfield of the Kirchhoff vortex is used to verify the results from the vortex particle method used in this study, and Eq. (2) is used as a base model to estimate sound emission frequencies from different types of aircraft and to verify the results from the far-field vortex sound formula presented in the Appendix.

III. Case Studies for Out-of-Ground Vortex Wake Without Background Flow

Table 1 lists the majority aircraft types and their configurations (related to the wake vortex behavior) whose wake vortex sound was measured during the 2003 phased array test at Denver International Airport [13,18]. The wake sound emission frequencies are calculated based on the Kirchhoff vortex model. The wake vortex span is estimated as 78.5% of the wing span according to a typical elliptical wing loading. The circulation is calculated approximately from a uniform aircraft landing weight at 80% maximum landing weight with fixed approach speed. Although it is difficult to accurately estimate the vortex core size, a reasonable range of the core radius is from 1.5 to 2% wing span according to the field measurement data [36]. A median core radius in between this range is selected as 1.65% of wingspan. With the relation of $\Omega = \Gamma/a^2$, the acoustic frequency of a Kirchhoff single vortex can be calculated as $f = \Omega/4\pi$. The lower bounds (LB), median, and upper bounds (UB) frequencies correspond, respectively, to the core radii of 2, 1.65, and 1.5% wing span. The last column of Table 1 is the results of computational simulation for the wake vortices modeled as a pair of counterrotating vortices initially as Kirchhoff vortices with a median core size (1.65% wing span). The simulation procedure is explained in the next section. It can be seen in Table 1 that the acoustic frequencies from the numerical results are almost exactly the same as that predicted by a single Kirchhoff vortex model using Eq. (2). This is due to the fact that the two vortex cores are relatively far away because of the small radii of the cores. Therefore, the mutual induction effect between the two vortices is relatively small and does not influence the vortex-core rotating frequency. When the vortices are closer each other, the ratio between the core size and the vortex distance influences the sound frequency, a point that was also made in Tang and Ko's work [23], but needs to be further explored in the future research.

The acoustic frequencies vs the wing spans in Table 1 are plotted in Fig. 1. By grouping the aircraft types into small regional jets (RJs) and large jets, a general trend can be observed that shows that wake acoustics from large aircraft has an inverse relation between peak frequency and wing span. Small aircraft do not follow such a relation, which could be a reflection of a relatively wider range of aircraft design parameters for small aircraft than those for large aircraft. Comparisons of this predicted trend with the field measurement data also provide evidences to confirm the relation for the large aircraft.

In Fig. 2, measured data are plotted for two cases of B737 and two cases of B757. Details of the measurement and data reduction procedure are described elsewhere [37,38]. In these measurements, one nondimensional time unit is the approximate time for the vortex pair to descend one vortex span [20], and is equal to $2\pi b_o^2/\Gamma$, where b_o and Γ are, respectively, the initial vortex span and circulation. In each case, the data within the measurement period of second nondimensional time are selected for comparison because it has the

Table 1 Aircraft types and configurations and estimated wake frequencies based on the Kirchhoff vortex model

Aircraft type		Wing span b, m	Wake vortex span b_o, m	Circulation gamma, m^2/s	Min core radius $1.5\%b$, m	Median core radius $1.65\%b$, m	Max core radius $2\%b$, m	LB acoustic freq. (single), Hz	Median acoustic freq. (single), Hz	UB acoustic freq. (single), Hz	Half of vortex span L, m	Maximum rotating speed, m/s	Numerical median freq. (pair), Hz
Airbus	A318	34.15	26.82	252.68	0.51	0.56	0.68	13.72	20.16	24.40	13.41	71.38	20.20
	A319	34.15	26.82	265.77	0.51	0.56	0.68	14.43	21.21	25.66	13.41.	75.08	21.25
	A320	34.15	26.82	274.72	0.51	0.56	0.68	14.92	21.92	26.53	13.41	77.61	21.96
	A321	34.15	26.82	266.76	0.51	0.56	0.68	14.49	21.29	25.76	13.41	75.36	21.33
	A343	60.06	47.17	458.12	0.90	0.99	1.20	8.04	11.82	14.30	23.59	73.58	11.84
Boeing	B717	28.35	22.27	235.57	0.43	0.47	0.57	18.56	27.26	32.99	11.13	80.14	27.31
	B737	28.96	22.75	281.74	0.43	0.48	0.58	21.27	31.25	37.81	11.37	93.83	31.31
	B738	34.45	27.06	262.06	0.52	0.57	0.69	13.98	20.54	24.86	13.53	73.37	20.58
	B757	38.11	29.93	347.95	0.57	0.63	0.76	15.17	22.29	26.97	14.97	88.07	22.33
	B767	47.56	37.35	377.17	0.71	0.78	0.95	10.56	15.51	18.77	18.68	76.49	15.54
	B777	60.67	47.65	456.62	0.91	1.00	1.21	7.86	11.54	13.97	23.83	72.60	11.56
MD	MD80	32.93	25.86	240.32	0.49	0.54	0.66	14.04	20.62	24.95	12.93	70.40	20.66
	MD90	32.93	25.86	276.26	0.49	0.54	0.66	16.14	23.71	28.69	12.93	80.93	23.75
Regional	B190	17.68	13.89	70.93	0.27	0.29	0.35	14.36	21.11	25.54	6.94	38.69	21.15
	CRJ2	21.04	16.52	139.14	0.32	0.35	0.42	19.91	29.25	35.40	8.26	63.80	29.31
	BA46	26.22	20.59	283.17	0.39	0.43	0.52	26.08	38.32	46.37	10.30	104.18	38.40
	DH8B	25.91	20.35	144.55	0.39	0.43	0.52	13.63	20.03	24.23	10.18	53.81	20.06
	E120	25.91	20.35	101.14	0.39	0.43	0.52	9.54	14.01	16.95	10.18	37.65	14.04

full time history of the measured data and is considered more accurate from the measurement point of view, although the data at the first and the third nondimensional time periods did show similar behaviors. The solid and dashed lines represent the wake vortex and background power spectral densities, respectively. The black dots indicate the predicted frequency peaks based on the numerical simulation values in Table 1 for the median frequency values. It can be seen from Fig. 2 that near the peak frequencies there is a significant detectable wake power above background acoustic noise, although the measured power spectral levels shown here are related to the microphone-array gain from the beam-forming process [37,38] instead of the direct measure of sound-pressure levels. The measured and theoretically predicted peak frequency values have a very good agreement.

Figure 2 also shows that the measured B757 wake peak frequencies are lower than those of B737, which confirms the trend predicted in the calculations based on the Kirchhoff vortex model. These results suggest that the Kirchhoff vortex core could be the mechanism responsible for the peaks observed in the measured spectra. It should be pointed out that the comparisons of experimental results with the theory should focus on the trend, instead of the absolute values because the theoretical calculation requires input parameters that are very often not easily measured with high certainties of accuracy, such as the vortex span, core size, and shape.

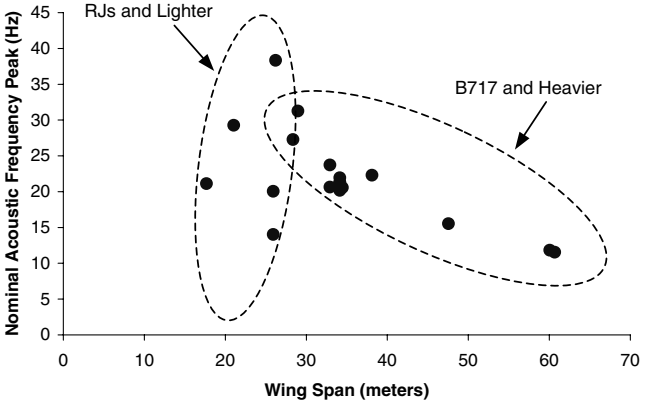

Fig. 1 Acoustic frequencies vs the wing spans for different types of aircraft.

IV. Numerical Simulation Cases

Whereas the analytical solution of the Kirchhoff vortex model used in the preceding sections is for a single vortex in an infinite domain, aircraft vortex wakes actually consist of a pair of counterrotating vortices for which the analytical solution does not exist. In addition, ground effects and atmospheric conditions can further complicate the matter to pose a question on the predictions using the Kirchhoff vortex model. Therefore, for realistic vortex wake cases, numerical solutions are needed and discussed in this section.

Using the vortex half-span as the characteristic length and the nominal maximum rotating speed at the outer edge of the vortex core, $a\Omega/2$, as the characteristic velocity, the simulation equations can be nondimensionalized for computational purposes. The simulation procedure is developed using a vortex particle method [33]. At the beginning of the simulation, the initially specified Kirchhoff vortices have the parameters of $a = 0.042$, $\epsilon = 0.05$, and $\Omega = 47.69$, for the median core-size (1.65% wing span) vortices. The vortex particles are distributed on a grid mesh with the grid size of $\Delta x = \Delta y = 1.68 \times 10^{-3}$ and a particle core parameter α of $2\Delta x$ [24]. This gives 50 vortex particles in a nominal vortex-core diameter of $2a$. Such a fine grid solution selected in the simulation is to ensure proper resolution for the vorticity field to correctly capture the core rotation frequency. Simulation tests with lower resolution have shown that the acoustic frequency numerically shifts to lower values. The required high resolution in this problem poses difficulties in using the Eulerian type of simulation with which only high-order accuracy schemes with high grid resolution are able to capture the frequency correctly [39]. Unfortunately, the small core radii in the wake vortices, in comparison to the distance between the vortices, limited the resolution required for the Eulerian Navier–Stokes simulation [40]. The reason is because on one hand, the domain has to be sufficiently large to include the large distance between the two vortices so that the numerical domain-boundary effect is reduced to a minimal. On the other hand, the numerical grid size has to be sufficiently small to resolve the small vortex cores. This situation results in an excessive number of computational grid points that is difficult to accommodate even with today's state-of-the-art supercomputers.

It is noted that the selected small value of ϵ for the initial vortices is to satisfy the requirement of $\epsilon \ll 1$ for a Kirchhoff vortex. As the vortices are allowed to freely evolve following the governing equations at the later times, the selection of this initial value need not be precise. There are no measured data available for determining the eccentricity of a vortex. Whereas the wake vortices mostly result

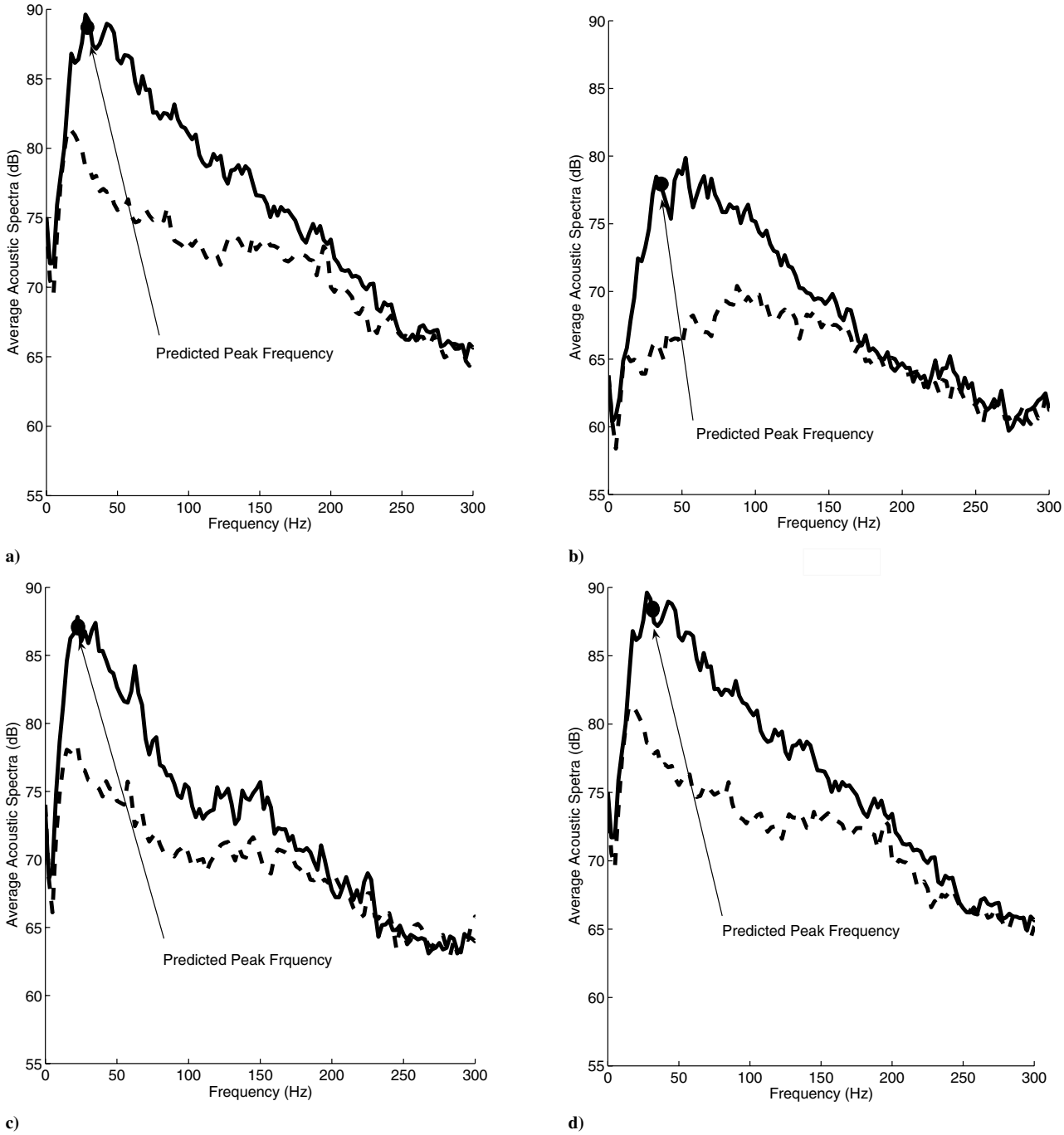

Fig. 2 Measured wake acoustic spectra for B737 and B757, and comparisons of measured peak frequencies with the predicted frequencies using the Kirchhoff vortex model. The solid and dashed lines represent the wake vortex and background power spectral densities, respectively. The black dots indicate the predicted frequency peaks based on the numerical simulation: a) B737-800, b) B737, c) B757, d) B757.

from shear-layer instability and multiple vortex merging, numerical simulations from our study on these phenomena have shown that the resultant vortices have a stable nominal eccentricity approximately 0.1–0.2. This supports the argument that the sound mechanism described here is persistent.

The initial distribution of vorticity is

$$\zeta(\boldsymbol{x} - t) = \sum_n \Gamma_n g_\alpha[\boldsymbol{x} - \boldsymbol{x}_n(t)] \tag{3}$$

where Γ_n is the circulation of each vortex particle defined as $(\Delta x)^2\Omega$ in the Kirchoff vortex model here, and g_α is a second-order particle core function [33] defined as

$$g_\alpha(\boldsymbol{x}) = \frac{1}{\pi\alpha^2}\exp(-|\boldsymbol{x}|^2/\alpha^2) \tag{4}$$

The size of time step is $\Delta t = 5.1465 \times 10^{-3}$, which is equal to $10T/512$, where T is the oscillation period of a single Kirchhoff vortex equal to $4\pi/\Omega$. By carrying out simulation of 512 time steps, a time history of 10 periods is covered. This time step is sufficiently small to resolve the frequency content related to the core vorticity in this case. During the simulation, remeshing is done at each time step.

For modeling the wake vortex system, a counterrotating vortex pair composed of two opposite-sign Kirchhoff vortices is used as the initial condition to represent the vortex wake out-of-ground effect. For in-ground-effect cases, the effect of an image pair of the wake vortices at the other side of the ground boundary is included to represent the inviscid ground effect. Effects of wind shear are also simulated under moderate and strong shear conditions to be discussed later in this section. In these different simulation cases, different domain sizes and moving domains are used to maintain a

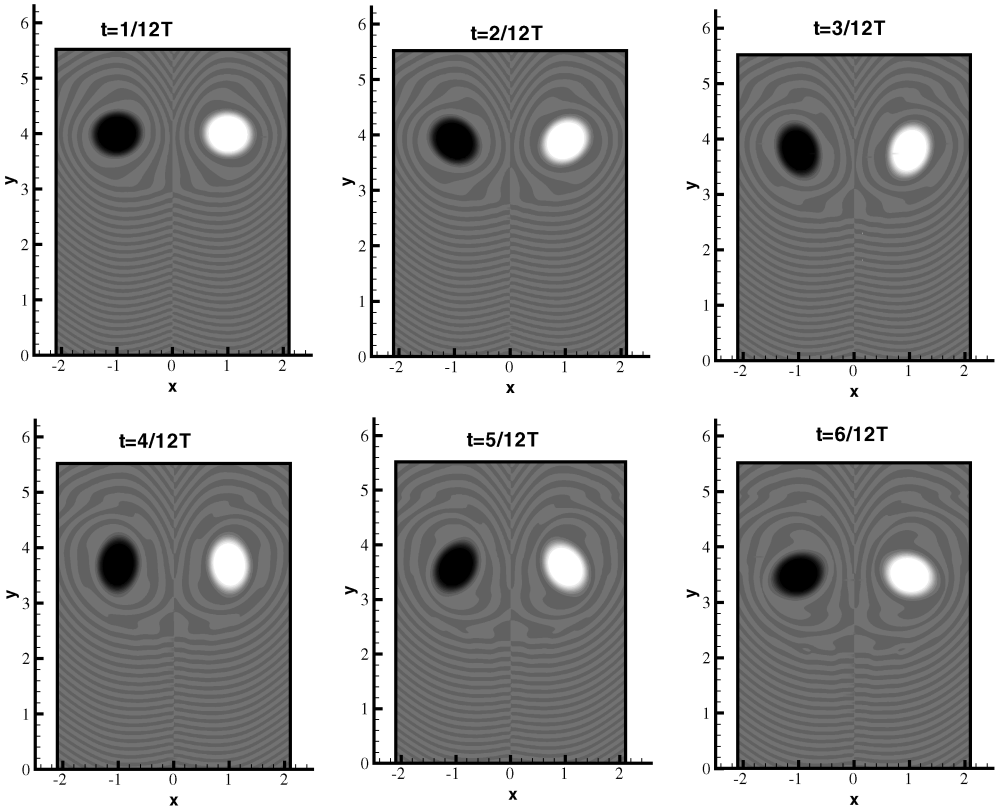

Fig. 3 Illustration of the history of contours of the vortex wake represented by a pair of out-of-ground wake vortices initiated as a pair of counterrotating Kirchhoff vortices.

proper spatial resolution around the vortex core. In each case, the meshed domain that covers the vortex core is at least twice of the core size, to ensure that the vorticity particles distributed on the mesh sufficiently include all the vorticity field in the core region.

Figure 3 is an illustration of the history of vorticity contours for interactions of a pair of wake vortices not in ground effect. Notice in this figure large vortex cores are used to illustrate their forms, and the shown domain size is truncated from the real domain used in the simulation for illustration purposes. The history corresponds to a half period of the Kirchhoff vortex rotation. The light-color vortex is a counterclockwise vortex with its elliptical core also rotating counterclockwise, and the dark-color vortex is a clockwise vortex with its elliptical core also rotating clockwise. It can be seen that it is this asymmetric "churning" effect of the solid-body-like rotation motion of the elliptical-shaped vortex cores that causes the unsteady fluid flow responsible for the far-field acoustics. This effect, caused by the eccentricity in an elliptical vortex core, is essential to generation of acoustic signal, because a perfectly round vortex does not produce sound, as stated previously in Sec. II. Again, although the initial elliptical vortex cores are allowed to deform in the later times, the basic elliptical shapes persist throughout the whole history, producing a persistent sound source.

Whereas Eq. (2) gives acoustic pressure from a single Kirchhoff vortex, for a system of discrete vortices such as the wake vortex system, an extended far-field acoustic pressure formula is needed to attribute its source to the near-field unsteady interactions of multiple vortices. A matched-asymptotic-expansion method [21,41] has been used that matches the inner region of incompressible vortex flow to the outer region of acoustic field. Whereas previous research only considered the dipole-type sources, in the vortex-core problem only quadrupole noise is generated as shown in Eq. (2). Therefore a higher-order expansion than those previously derived [21,41] is needed for the near field. The detailed derivation and the equations used for the far-field acoustic pressure calculation for a discrete vortex system are provided in the Appendix. In the far-field acoustic pressure calculation in the simulation, Eq. (A11) in the Appendix is used. For the purpose of this study, the far-field location for calculating acoustic pressure is placed at a distance of 10 characteristic lengths ($r = 10$) in the flyover direction ($\theta = 90$ deg) under the wake vortex pair. A nominal Mach number of 0.27 is specified in the calculation.

Figure 4 compares the simulated dimensionless spectrum of the far-field acoustic pressure calculated using Eq. (A11). It should be noted that in several cases considered here, the second quadrupole term in Eq. (A11), the $\Gamma_j(x_j^2 - y_j^2)$ term, turns out to be zero because of the vorticity symmetry in the flowfield. However, in other more general cases when the symmetry no longer exists, this term is not zero. Figure 4a compares the single Kirchhoff vortex with the counterrotating vortex pair, and Fig. 4b compares the single Kirchhoff vortex with the counterrotating vortex pair in ground effect. It can be seen that in all the cases, there exists a significant peak at the dimensionless frequency of $f = 3.8$, which is exactly related to the vorticity value in the Kirchhoff vortex core as $\Omega/4\pi$, as shown in the analytical solution of Eq. (2). This means that in the vortex wake, the sound generation mechanism due to vortex-core rotation is not influenced by the macroscopic vortex interactions, as long as the distances between the vortices are large in comparison with the core size.

Figure 5 is plotted to compare the effect of vortex-core size. A case with an elliptical vortex-core size of $a = 0.084$ is compared with the original core size of $a = 0.042$, with the same vorticity of 47.69 inside the core. It can be seen that the peak frequency still remains at $f = 3.8$. The magnitude of the spectrum is increased due to the increase of the core size with the same vorticity, because the total circulation, which is equal to the vorticity times the core area, is increased. This phenomenon agrees with what shows in Eq. (2), where the frequency of the acoustic pressure only depends on the vorticity level ($\Omega/2$), and the magnitude of the acoustic pressure is increased due to the increase of the core size a. Whereas Eq. (2) is for a single Kirchhoff vortex, the results in Fig. 5 also show that even when the core size is doubled in the wake vortices (with the ratio of core radius to vortex distance to be 0.084 now), the wake sound emission behavior remains the same as that of a single Kirchhoff vortex.

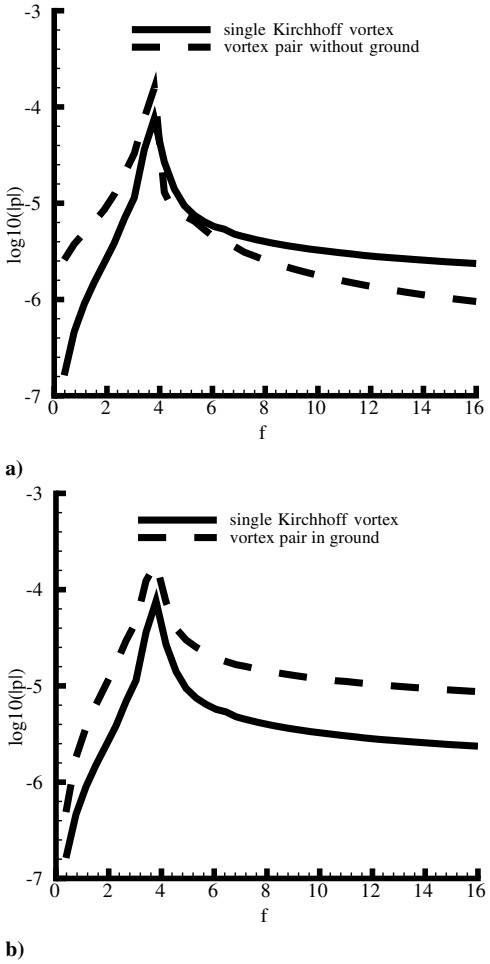

Fig. 4 a) Comparison of simulated dimensionless spectrum of acoustic pressure between that of a single Kirchhoff vortex and that of a pair of counterrotating vortices; b) comparison of simulated dimensionless spectrum of acoustic pressure between that of a single Kirchhoff vortex and that of a pair of counter-rotating vortices with the ground image.

It can be argued that under realistic atmospheric conditions, wind shear and turbulence, in the form of rotational straining fields, can impose significant effects on the wake vortex-core dynamics. There are several ways to simulate these effects. One way is to represent the background field with vorticity field and directly simulate the wake vortices along with the background vortices. Although this method is able to directly simulate the interactions between background shear and the wake vortices, it is computationally expensive because a large number of vortices need to be distributed all over the computational domain to represent the background flow. Another way is to split the wake vortex flow from the background flow.

For the vorticity transport equation of 2-D inviscid incompressible flow,

$$\frac{\mathrm{D}(\bar{\Omega}+\Omega)}{\mathrm{D}t}=\frac{\partial(\bar{\Omega}+\Omega)}{\partial t}+(\bar{u}_j+u_j)\frac{\partial(\bar{\Omega}+\Omega)}{\partial x_j}=0 \tag{5}$$

the flow variables can be split into the background flow $(\bar{\Omega},\bar{\Omega}_j)$ and the induced part by wake vortices (Ω,u_j). Neglecting the influence from wake vortices on background flow, the background flow itself satisfies

$$\frac{\mathrm{D}\bar{\Omega}}{\mathrm{D}t}=\frac{\partial\bar{\Omega}}{\partial t}+\bar{u}_j\frac{\partial\bar{\Omega}}{\partial x_j}=0 \tag{6}$$

Substituting Eq. (6) into Eq. (5) results in

$$\frac{\mathrm{D}\Omega}{\mathrm{D}t}=\frac{\partial\Omega}{\partial t}+(\bar{u}_j+u_j)\frac{\partial\Omega}{\partial x_j}=-u_j\frac{\partial\bar{\Omega}}{\partial x_j} \tag{7}$$

If we only consider a constant-shear crossflow, which flow satisfies Eq. (6), Eq. (7) then becomes

$$\frac{\mathrm{D}\Omega}{\mathrm{D}t}=\frac{\partial\Omega}{\partial t}+(\bar{u}_j+u_j)\frac{\partial\Omega}{\partial x_j}=0 \tag{8}$$

Therefore, the wake vortices can be treated as a pair of vortices transported at a velocity of background wind plus the induced velocity due to wake vortices. The vortex particle method can be easily implemented as

$$\frac{\mathrm{d}\Gamma_p}{\mathrm{d}t}=0 \tag{9}$$

$$\frac{\mathrm{d}\boldsymbol{X}_p}{\mathrm{d}t}=\bar{\boldsymbol{u}}_p+\boldsymbol{u}_p=\bar{\boldsymbol{u}}_p+\sum_q K_\alpha(\boldsymbol{X}_p-\boldsymbol{X}_q)\Gamma_q \tag{10}$$

where Γ_p is the circulation of each vortex particle, and K_α is defined as

$$K_\alpha(\boldsymbol{X})=\frac{\boldsymbol{X}\times\boldsymbol{k}}{2\pi|\boldsymbol{X}|}[1-\exp(-|\boldsymbol{X}|^2/\alpha)] \tag{11}$$

and the vortex particle core parameter α is selected in Eq. (4).

Figures 6 and 7 compare cases of a wake vortex pair in a constant-shear background flow with that of a single Kirchhoff vortex. The vortices are initiated by the same parameters as mentioned before. In

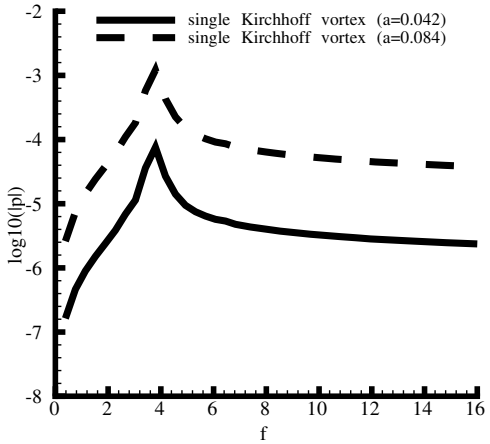

Fig. 5 Comparison of simulated dimensionless acoustic pressure spectra of two different core sizes of Kirchhoff vortices with the same vorticity value inside their cores.

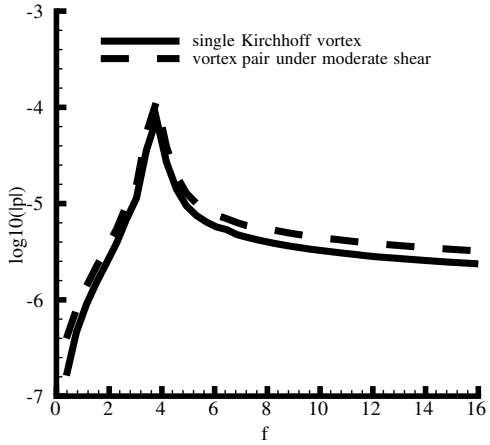

Fig. 6 Comparison of dimensionless acoustic pressure spectra of the wake vortex pair under a moderate constant shear with that of a single Kirchhoff vortex.

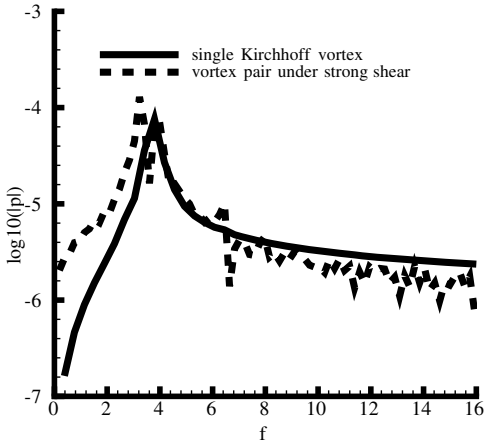

Fig. 7 Comparison of dimensionless acoustic pressure spectra of the wake vortex pair under a strong constant shear with that of a single Kirchhoff vortex.

Fig. 6 the level of shear vorticity is 0.01, and in Fig. 7 it is 0.1. For a B757, these shear strengths represent a crosswind speed increase of 0.06 m/s per meter and 0.06 m/s per meter, respectively. Therefore for a B757, the case represented in Fig. 6 is considered a moderate shear because the shear condition is very close to the cases of run 7 and run 9 in [3]. The case represented in Fig. 7 is an unusually strong shear that can only occur locally and last a short period of time in the practical atmosphere. Figure 6 shows that under moderate shear, the dominant frequency again remains the same as that of the core rotation of a single Kirchhoff vortex. Under strong shear in Fig. 7, the peak frequencies can be slightly shifted due to shear/vortex-core interactions. It seems one peak is slightly higher than the original frequency of a single vortex and the other is shifted slightly lower. These two peaks can be attributed to the two counterrotating vortices in the vortex pair, one with strengthened vorticity and the other with weakened vorticity. Whereas the total circulation remains the same in each of the vortices as guaranteed by Eq. (9), the vorticity level changes are caused by deformation of the cores. The background shear, if carrying vorticity of the positive sense in the simulation, deforms and expands the negative vortex core, and at the same time increases its eccentricity, resulting in a lower frequency but higher sound level peak in Fig. 7. The same shear tends to shrink the positive vortex core and decreases the eccentricity, resulting in a higher frequency but lower sound level peak. Figure 7 supports the argument that each peak is caused by a corresponding Kirchhoff vortex-core rotation. With other effects such as background turbulence, the shifted two peaks may get smeared into one broader hump such as those shown in the measured data in Fig. 2.

It needs to be pointed out that the purpose of the study is to identify the most unique and consistent mechanism associated with the vortex. This mechanism is related to the portion of the spectra that shows up as a hump above the background in the measurement data as in Fig. 2. It does not mean that there are no useful frequency content above or below such a hump. Although the higher frequency above the range of the rotating core frequency can be used and do show up in the source localization process [12,15,18,38], the acoustic energy is, however, weak compared to that of the core-dynamics-based mechanism, and it does not appear to be as consistently above the atmospheric noise background.

V. Conclusions

Both measurement data and theoretical results indicate a mechanism of sound emission of aircraft wake vortices due to the self-induction rotation of the elliptic vortex core. There is a dominant frequency of sound pressure that matches the rotation frequency of a Kirchhoff vortex-core rotation. Calculated results based on this mechanism using realistic aircraft configurations show that wake acoustics from large aircraft has an inverse relation between peak frequency and wing span. Small aircraft do not follow such a relation. By looking into a particular set of data for B757 and B737, both the measurement and the calculation agree that the B757 wake peak frequencies are lower than those of B737. When the wake vortices are initialized by counterrotating Kirchhoff vortices, numerical simulations based on the inviscid vortex particle method confirm that the frequency of the wake sound emission remains essentially the same as that of the classical Kirchhoff vortex, even under the influences of an inviscid ground effect and a moderate, constant-shear cross wind. These results suggest that the identified sound generation mechanism attributed to the vortex core dynamics should be a robust acoustic radiation mechanism, a promising wake indicative among a number of active sound generation processes involved in aircraft vortex wakes.

Appendix: Far-Field Sound Formula for a Discrete Vortex System

Because the inner region flowfield is generated by a system of discrete vortices, the complex velocity potential can be expressed as

$$W = \Phi + i\Psi = \frac{i}{2\pi}\Gamma_j(t)\,\ell_n[z - z_j(t)] \tag{A1}$$

where Γ_j is the jth vortex circulation at position z_j, and z is the far-field location. Both Γ_j and z_j can be functions of time. The Einstein summation convention, with respect to j, is implied. After expanding the logarithmic function in Eq. (A1) under the condition of $|z_j/z| \ll 1$, we have

$$W = \frac{i}{2\pi}\ell_n z\sum_j \Gamma_j - \frac{i}{2\pi}\Gamma_j\frac{z_j}{z} - \frac{i}{4\pi}\Gamma_j\frac{z_j^2}{z^2} + \mathcal{O}\left[\left(\frac{z_j}{z}\right)^3\right] \tag{A2}$$

The first term does not relate to acoustic sources, and is steady following Kelvin's theorem. Denoting the fluctuation complex velocity potential as w, we have

$$w = -\frac{i}{2\pi z}\Gamma_j z_j - \frac{i}{4\pi}\Gamma_j\frac{z_j^2}{z^2} \tag{A3}$$

By means of the linearized Bernoulli equation in nondimensional form, the inner pressure fluctuation is

$$p_i = -\frac{\partial\phi}{\partial t} = \frac{1}{2\pi r}\left[\frac{\mathrm{d}(\Gamma_j x_j)}{\mathrm{d}t}\sin\theta - \frac{\mathrm{d}(\Gamma_j y_j)}{\mathrm{d}t}\cos\theta\right] - \frac{1}{4\pi r^2}\left\{\frac{\mathrm{d}}{\mathrm{d}t}[\Gamma_j(2xy)_j]\cos(2\theta) - \frac{\mathrm{d}}{\mathrm{d}t}[\Gamma_j(x_j^2 - y_j^2)]\sin(2\theta)\right\} \tag{A4}$$

where $r = |z|$ and $\theta = Arg(z)$ are the distance and angle of the far-field receiver, respectively, and are assumed independent of time.

The pressure fluctuation at the outer region, p_o, satisfies the convective wave equation

$$\frac{\partial^2 p_o}{\partial x^2} + \frac{\partial^2 p_o}{\partial y^2} - M^2\frac{\mathrm{D}^2 p_o}{\mathrm{D}t^2} = 0 \tag{A5}$$

After transformation using the outer variables and letting $M \to 0$, an acoustic equation is obtained

$$\frac{\partial^2 p_o}{\partial X^2} + \frac{\partial^2 p_o}{\partial Y^2} - \frac{\partial^2 p_o}{\partial t^2} = 0 \tag{A6}$$

where $X = Mx$ and $Y = My$. The format of the outer solution is suggested by the inner solution to be

$$p_o = \sum_j S_j(R,t)\sin\theta + \sum_j C_j(R,t)\cos\theta + \sum_j K_j(R,t)\cos 2\theta + \sum_j L_j(R,t)\sin 2\theta \tag{A7}$$

where $R = Mr$, and S_j, C_j, K_j, and L_j are functions to be determined.

After substituting this expression into Eq. (A6) and performing the Fourier transform in time, Eq. (A6) can be solved to yield p_o in the frequency domain for the outgoing waves,

$$\hat{p}_o = \left(\sum_j A_j \sin\theta + \sum_j B_j \cos\theta\right) H_1^{(2)}(\omega R), + \left(\sum_j E_j \cos 2\theta + \sum_j G_j \sin 2\theta\right) H_2^{(2)}(\omega R) \tag{A8}$$

where $H_1^{(2)}$ is the second-kind Hankel function of order one, $H_2^{(2)}$ is the second-kind Hankel function of order two, ω is the frequency, and A_j, B_j, E_j, and G_j are to be determined by the matching condition between the inner and outer solutions.

The matching is performed by letting $R \to 0$ in Eq. (A8) and rewriting the expression in terms of the inner variables. Because

$$H_1^{(2)}(\omega R \to 0) \to \frac{2i}{\pi\omega R} = \frac{2i}{\pi\omega M r} \tag{A9}$$

and

$$H_2^{(2)}(\omega R \to 0) \to \frac{4i}{\pi(\omega R)^2} = \frac{4i}{\pi\omega^2 M^2 r^2} \tag{A10}$$

substituting these expressions into Eq. (A8) and comparing with Eq. (A4) yields the outer solution as

$$\hat{p}_o = -i\frac{M\omega}{4} H_1^{(2)}(\omega R) \sum_j \left\{ \boldsymbol{F}\left[\frac{\mathrm{d}(\Gamma_j x_j)}{\mathrm{d}t}\right] \sin\theta - \boldsymbol{F}\left[\frac{\mathrm{d}(\Gamma_j y_j)}{\mathrm{d}t}\right] \cos\theta \right\} + i\frac{M^2\omega^2}{16} H_2^{(2)}(\omega R) \sum_j \left\{ \boldsymbol{F}\left[\frac{\mathrm{d}(2\Gamma_j x_j y_j)}{\mathrm{d}t}\right] \cos 2\theta - \boldsymbol{F}\left[\frac{\mathrm{d}[\Gamma_j (x_j^2 - y_j^2)]}{\mathrm{d}t}\right] \sin 2\theta \right\} \tag{A11}$$

where $\boldsymbol{F}[\,]$ denotes the Fourier transform in time. Note that Eq. (A11) is a dimensionless expression for far-field acoustic pressure. The characteristic parameters used in the expression are vortex half-span L, nominal maximum vortex rotating speed U, and the density of air ρ_o.

With only the quadrupole source from the vortex core, the dipole terms (related to $\sin\theta$ and $\cos\theta$) in Eq. (A11) are zero. The strengths of the quadrupole terms depend on $\Gamma_j x_j y_j$ and $\Gamma_j (x_j^2 - y_j^2)$, a fact that agrees with those expressions for 2-D vortex systems by Mohring [45,46] and others [22,34,42–44,47].

Acknowledgments

The authors wish to express their appreciation to the NASA's Aeronautics Research Mission Directorate, and in particular the Airspace Systems Program, for funding the exploration of this fundamental mechanism for detecting aircraft wakes, and to the program manager, Wayne Bryant, for ensuring that the work focused on addressing the core issues. The first and second authors were funded under NNL04AA77G. We also thank John Dunkel of USDOT Volpe Center for generating the experimental results plots.

References

[1] *Aeronautical Information Manual: Official Guide to Basic Flight Information and ATC Procedures*, Federal Aviation Administration, Washington, DC, Feb. 2006.

[2] Critchley, J. B., and Foot, P. B., "United Kingdom Civil Aviation Authority Wake Vortex Database: Analysis of Incidents Reported Between 1972 and 1990," *Proceedings of the FAA International Wake Vortex Symposium*, edited by J. N. Hallock, DOT/FAA/SD-92/1.1, Washington, DC, June, 1992, pp. 8-1–8-17.

[3] Ash, R. L., and Zheng, Z. C., "Numerical Simulations of Commercial Aircraft Wakes Subjected to Airport Surface Weather Conditions," *Journal of Aircraft*, Vol. 35, No. 1, 1998, pp. 18–26.

[4] Han, J., Lin, Y., Arya, S. P., and Proctor, F. H., "Numerical Study of Wake Vortex Decay and Descent in Homogeneous Atmospheric Turbulence," *AIAA Journal*, Vol. 38, No. 4, 2000, pp. 643–656.

[5] Zheng, Z. C., "The Betz Invariants and Generalization of Vorticity Moment Invariants," *AIAA Journal*, Vol. 39, No. 3, pp. 431–437.

[6] Zheng, Z. C., and Ash, R. L., "A Study of Aircraft Wake Vortex Behavior Near the Ground," *AIAA Journal*, Vol. 34, No. 3, 1996, pp. 580–589.

[7] Zheng, Z. C., and Baek, K., "Inviscid Interactions Between Wake Vortices and Shear Layers," *Journal of Aircraft*, Vol. 36, No. 2, 1999, pp. 477–480.

[8] Zheng, Z. C., and Lim, S. H., "Validation and Operation of a Vortex-Wake/Shear Interaction Model," *Journal of Aircraft*, Vol. 37, No. 6, 2000, pp. 1073–1078.

[9] Hardin, J. C., and Wang, F. Y., "Sound Generation by Aircraft Wake Vortices," NASA CR-2003-212674, Dec. 2003.

[10] Bedard, A. J., Jr., "Low-Frequency Atmospheric Acoustic Energy Associated with Vortices Produced by Thunderstorms," *Monthly Weather Review*, Vol. 133, No. 1, 2005, pp. 241–263.

[11] Alix, D. C., Simich, P. D., Wassaf, H., and Wang, F. Y., "Acoustic Characterization of Wake Vortices in Ground Effect," AIAA Paper 2005-0260, Jan. 2005.

[12] Booth, E. R., Jr., and Humphreys, W. M., Jr., "Tracking and Characterization of Aircraft Wakes Using Acoustic and Lidar Measurements," AIAA Paper 2005-2964, May 2005.

[13] Dougherty, R. P., Wang, F. Y., Booth, E. R., Watts, M. E., Fenichel, N. and D'Errico, R. E., "Aircraft Wake Vortex Measurements at Denver International Airport," AIAA Paper 2004-2880, May 2004.

[14] Fine, N. E., and Kring, D. C., "Opto-Acoustic Tracking of Aircraft Wake Vortices," AIAA Paper 2005-2965, May 2005.

[15] Michel, U., and Bohning, P., "Investigation of Aircraft Wake Vortices with Phased Microphone Arrays," AIAA Paper 2002-2501, June 2002.

[16] Qiao, W., and Michel, U., "A Study on the Vortex Shedding Noise from the Wake of Aircraft Wings," AIAA Paper 2000-1973, June 2000.

[17] Rubin, W. L., "The Generation and Detection of Sound Emitted by Aircraft Wake Vortices in Ground Effect," *Journal of Atmospheric and Oceanic Technology*, Vol. 22, May 2005, pp. 543–554.

[18] Wang, F. Y., Wassaf, H. S., Gulsrud, A., Delisi, D. P. and Rudis, R. P., "Acoustic Imaging of Aircraft Wake Vortex Dynamics," AIAA Paper 2005-4849, June 2005.

[19] Powell, A., "Theory of Vortex Sound," *Journal of the Acoustical Society of America*, Vol. 36, No. 1, 1964, pp. 177–195.

[20] Greene, G. C., "An Approximate Model of Vortex Decay in the Atmosphere," *Journal of Aircraft*, Vol. 23, No. 7, 1986, pp. 566–573.

[21] Zheng, Z. C., "Far-Field Acoustic Pressure from a System of Discrete Vortices with Time-Varying Circulation," AIAA Paper 2005-3005, May 2005.

[22] Tang, S. K., and Ko, N. W. M., "Basic Sound Generation Mechanisms in Inviscid Vortex Interactions at Low Mach Number," *Journal of Sound and Vibration*, Vol. 262, No. 1, 2003, pp. 87–115.

[23] Tang, S. K., and Ko, N. W. M., "Sound Sources in the Interactions of Two Inviscid Two-Dimensional Vortex Pairs," *Journal of Fluid Mechanics*, Vol. 419, Sept. 2000, pp. 177–201.

[24] Eldredge, J. D., "The Acoustics of Two-Dimensional Leapfrogging Vortices," AIAA Paper 2005-2954, May 2005.

[25] Inoue, O., "Sound Generation by the Leapfrogging Between Two Coaxial Vortex Rings," *Physics of Fluids*, Vol. 14, No. 9, 2002, pp. 3361–3364.

[26] Inoue, O., Hattori, Y., and Sasaki, T., "Sound Generation by Coaxial Collision of Two Vortex Rings," *Journal of Fluid Mechanics*, Vol. 424, Dec. 2000, pp. 327–365.

[27] Crow, S. C., "Stability Theory for a Pair of Trailing Vortices," *AIAA Journal*, Vol. 8, No. 12, 1970, pp. 2172–2179.

[28] Lamb, H., *Hydrodynamics*, 7th ed., Cambridge Univ. Press, Cambridge, England, 1975.

[29] Kopiev, V. F., and Chernyshev, S. A., "Vortex Ring Eigen-Oscillations as a Source of Sound," *Journal of Fluid Mechanics*, Vol. 341, June 1997, pp. 19–57.

[30] Saffman, P. G., *Vortex Dynamics*, Cambridge Univ. Press, Cambridge, England, 1995.

[31] Widnall, S. F., Bliss, D. B., and Tsai, C. Y., "The Instability of Short Wave on a Vortex Ring," *Journal of Fluid Mechanics*, Vol. 66, Pt. 1, 1974, pp. 35–47.

[32] Zheng, Z. C., "Thin-Tube Vortex Simulations for Sinusoidal Instability in a Counter-Rotating Vortex Pair," *International Journal for Numerical Methods in Fluids*, Vol. 39, No. 4, 2002, pp. 301–324.

[33] Cottet, G.-H., and Koumoutsakos, P., *Vortex Methods, Theory and Practice*, Cambridge Univ. Press, Cambridge, England, 2000.

[34] Howe, M. S., *Theory of Vortex Sound*, Cambridge Univ. Press, Cambridge, England, 2003.
[35] Rogers, M. M., and Moser, R. D., "The Three-Dimensional Evolution of a Plane Mixing Layer: The Kelvin-Helmholtz Rollup," *Journal of Fluid Mechanics*, Vol. 243, 1992, pp. 183–226.
[36] Delisi, D. P., Greene, G. C., Robins, R. E., Vicroy, D. C., and Wang, F. Y., "Aircraft Wake Vortex Core Size Measurements," AIAA Paper 2003-3811, June 2003.
[37] Wassaf, H. S., Ibe, O. C., Dougherty, R. P., and Zhang, Y., "Acoustical Spectral Analysis of a Wake Vortex Cross-Section Using Microphone-Arrays," *Journal of the Acoustical Society of America*, Vol. 117, No. 4, April 2005, p. 2546.
[38] Wassaf, H., Hardin, J., and Wang, F., "Atmospheric Effects on Microphone Array Analysis of Aircraft Vortex Sound," AIAA Paper 2006-2539, May 2006.
[39] Muller, B., and Yee, H. C., "High Order Numerical Simulation of Sound Generated by the Kirchhoff Vortex," *Computing and Visualization in Science*, Vol. 4, No. 3, 2002, pp. 197–204.
[40] Bohning, P., Baumann, R., Michel, U., and Gerz, T., "Numerical Study of Wake Vortex Noise Using LES and an Acoustic Analogy Method," *Euromech Colloquium 467: Turbulent Flow Noise Generation*, European Mechanics Society, July 2005.
[41] Kao, H. C., "Body-Vortex Interaction, Sound Generation, and Destructive Interference," *AIAA Journal*, Vol. 40, No. 4, 2002, pp. 652–660.
[42] Kambe, T., Minota, T., and Takaoka, T., "Oblique Collision of Two Vortex Rings and Its Acoustic Emission," *Physical Review E (Statistical Physics, Plasmas, Fluids, and Related Interdisciplinary Topics)*, Vol. 48, No. 3, 1993, pp. 1866–1881.
[43] Knio, O. M., Colorec, L., and Juve, D., "Numerical Study of Sound Emission by 2D Regular and Chaotic Vortex Configurations," *Journal of Computational Physics*, Vol. 116, No. 2, 1995, pp. 226–246.
[44] Mitchell, B. E., Lele, S., and Moin, P., "Direct Computation of the Sound from a Compressible Co-Rotating Vortex Pair," *Journal of Fluid Mechanics*, Vol. 285, 1995, pp. 181–202.
[45] Mohring, W., "On Vortex Sound at Low Mach Number," *Journal of Fluid Mechanics*, Vol. 85, 1978, pp. 685–691.
[46] Mohring, W., "Modelling Low Mach Number Noise," *Mechanics of Sound Generation in Flows*, edited by E.-A. Muller, Springer, New York, 1979.
[47] Muller, B., "On Sound Generation by the Kirchhoff Vortex," Uppsala University Report No. 209/1998, Department of Scientific Computing, Uppsala, Sweden, Oct. 1998.